Appl Phys B (2011) 102: 225–233
DOI 10.1007/s00340-010-4108-5

Applied Physics B
Lasers and Optics

Dynamic behavior of composite spectral Stokes singularities in superimposed partially coherent beams beyond the paraxial approximation

Y. Luo · B. Lü

Received: 9 April 2010 / Revised version: 14 May 2010 / Published online: 2 July 2010

Abstract The composite spectral Stokes singularities are introduced to describe polarization singularities in superimposed partially coherent beams beyond the paraxial approximation. Based on the vector Rayleigh–Sommerfeld diffraction integrals, the dynamic behavior of composite spectral Stokes singularities in the free-space propagation is studied and illustrated by numerical examples. A comparison with the previous work is also made.

1 Introduction

The polarization singularities in vector wavefields have attracted much interest and have been extensively studied analytically and experimentally since Nye's work [1] and that of many others [2–18]. Nye and Hajnal discovered polarization singularities for monochromatic electromagnetic wavefields in three dimensions, where the polarization becomes either linear (L-lines) or circular (C-lines). In general, the singular lines for the electric field and the magnetic field are different [2]. The theoretical predictions were first confirmed experimentally with microwaves [3]. Felde and Chernyshov et al. found the existence of the U (unpolarized) and P (completely polarized) singularities of paraxial combined beams assembled from mutually incoherent orthogonally polarized components [14, 17]. Schoonover and Visser studied the state of polarization of strongly focused radially polarized electromagnetic fields and showed that with a suitable change in the definition of the Stokes parameters the usual description of the state of polarization and polarization singularities in the paraxial case can be extended to the nonparaxial regime [12]. Based on the generalized Stokes parameters proposed by Korotkova and Wolf [19], we introduced the spectral Stokes singularities to describe the polarization singularities of partially coherent electromagnetic beams within the framework of the paraxial approximation [16]. On the other hand, Maleev and Swartzlander Jr. found that composite optical vortices may form when two or more beams interfere [20]. More recently, we have shown that there exist composite polarization singularities in superimposed fully coherent Lagurre–Gaussian beams beyond the paraxial approximation [18]. Singular Stokes-polarimetry as a new technique can find promising applications in metrology and inspection of polarized speckle fields [10, 15].

The purpose of the present paper is to study the dynamic behavior of polarization singularities in superimposed two off-axis partially coherent beams beyond the paraxial approximation. In accordance with [16, 18, 20], such polarization singularities can be referred to as composite spectral Stokes singularities. In Sect. 2, based on the vector Rayleigh–Sommerfeld diffraction integrals, the closed-form expression for the cross-spectral density matrix of superimposed partially coherent beams in the free-space nonparaxial propagation is derived, which enables us to express the spectral Stokes parameters and spectral complex fields in terms of the elements of the cross-spectral density matrix and to study the dynamic behavior of composite spectral Stokes singularities. Section 3 analyzes the composite spec-

Y. Luo (✉)
Department of Biomedical Engineering, Luzhou Medical College, Luzhou 646000, China
e-mail: luoluoeryan@126.com
Fax: +86-28-85412322

Y. Luo · B. Lü
Institute of Laser Physics & Chemistry, Sichuan University, Chengdu 610064, China

B. Lü
e-mail: baidalu0@tom.com

tral Stokes singularities by varying a controlling parameter, such as the spatial correlation length, ratio of waist width to wavelength, or off-axis distance. The dynamic evolution of composite spectral Stokes singularities in free space is dealt with in Sect. 4. Finally, Sect. 5 summarizes the main results obtained in this paper with a comparison to the previous work.

2 Theoretical formulation

The electric field of optical beams polarized in the x direction with vortex in the plane $z = 0$ reads as [20]

$$E_x(r, \varphi, 0) = E_0 \exp\left(-\frac{r^2}{w_0^2}\right) r^{|n|} \exp(in\varphi) \exp(i\beta), \tag{1a}$$

$$E_y(r, \varphi, 0) = 0, \tag{1b}$$

where E_0 is an amplitude constant, the background beam is assumed to be Gaussian with w_0 being the waist width, r, φ are the radial and azimuthal coordinates in the cylindrical coordinate system, n is the topological charge, and β is an arbitrary phase.

The 3×3 cross-spectral density matrix in the plane $z = 0$ takes the form [21]

$$W^0 = \begin{vmatrix} W_{xx}^0(\mathbf{r}_{01}, \mathbf{r}_{02}, 0) & 0 & 0 \\ 0 & 0 & 0 \\ 0 & 0 & 0 \end{vmatrix}, \tag{2}$$

with

$$W_{xx}^0(\mathbf{r}_{01}, \mathbf{r}_{02}, 0) = \left\langle E_x^*(\mathbf{r}_{01}, 0) E_x(\mathbf{r}_{02}, 0) \right\rangle, \tag{3}$$

where $\langle\,\rangle$ specifies the ensemble average and the asterisk denotes the complex conjugate, $r_{0\nu} = (r_{0\nu}, \varphi_{0\nu}) = (x_{0\nu}, y_{0\nu})$ ($\nu = 1, 2$, unless otherwise stated).

Assume that the statistical distribution of β corresponds to a Schell-model correlator [20, 22], from (1) and (3) we obtain

$$W_{xx}^0(r_{01}, r_{02}, 0) = E_{01} E_{02} \exp\left[-\frac{(\mathbf{r}_{01} - \mathbf{r}_{02})^2}{\sigma_0^2} - \frac{r_{01}^2 + r_{02}^2}{w_0^2}\right] \times (r_{01} r_{02})^{|n|} \exp\left[in(\varphi_2 - \varphi_1)\right], \tag{4}$$

where σ_0 denotes the spatial correlation length. For simplicity in the following we set $n = 1$.

Consider two parallel off-axis partially coherent vortex beams with off-axis distance vector $\mathbf{a}$ $(a, 0)$, i.e., $a_x = a > 0$, $a_y = 0$, where one beam is offset from the origin by a along the x axis and has topological charge $+1$, the other beam is offset by $-a$ along the x axis and has charge -1. The cross-spectral density matrix element W_{xx}^0 of the resulting beam in the plane $z = 0$ is expressed as [23]

$$\begin{aligned} &W_{xx}^0(\mathbf{r}_{01} - 2h_1\mathbf{a}, \mathbf{r}_{02} - 2h_2\mathbf{a}, 0) \\ &= \sum_{h_1=-\frac{1}{2}}^{\frac{1}{2}} \sum_{h_2=-\frac{1}{2}}^{\frac{1}{2}} \left\langle E_x^*(\mathbf{r}_{01} - 2h_1\mathrm{a}) E_x(\mathbf{r}_{02} - 2h_2\mathrm{a}) \right\rangle \\ &= \sum_{h_1=-\frac{1}{2}}^{\frac{1}{2}} \sum_{h_2=-\frac{1}{2}}^{\frac{1}{2}} W_0(\mathbf{r}_{01} - 2h_1\mathrm{a}, \mathbf{r}_{02} - 2h_2\mathrm{a}, 0). \end{aligned} \tag{5}$$

The vector Rayleigh–Sommerfeld diffraction integrals give the exact solutions of the Maxwell equations in the half space $z > 0$, and are expressed as [24]

$$E_x(\mathbf{r}) = -\frac{1}{2\pi} \iint_{z=0} E_x(\mathbf{r}_0, 0) \frac{\partial}{\partial z}\left[\frac{\exp(ikR)}{R}\right] d^2\mathbf{r}_0, \tag{6a}$$

$$E_y(\mathbf{r}) = -\frac{1}{2\pi} \iint_{z=0} E_y(\mathbf{r}_0, 0) \frac{\partial}{\partial z}\left[\frac{\exp(ikR)}{R}\right] d^2\mathbf{r}_0, \tag{6b}$$

$$\begin{aligned} E_z(\mathbf{r}) = \frac{1}{2\pi} \iint_{z=0} &\left[E_x(\mathbf{r}_0, 0) \frac{\partial}{\partial x}\left[\frac{\exp(ikR)}{R}\right] \right. \\ &\left. + E_y(\mathbf{r}_0, 0) \frac{\partial}{\partial y}\left[\frac{\exp(ikR)}{R}\right] \right] d^2\mathbf{r}_0, \end{aligned} \tag{6c}$$

where $\mathbf{r}_0 = x_0\mathbf{i} + y_0\mathbf{j}$, $\mathbf{r} = x\mathbf{i} + y\mathbf{j} + z\mathbf{k}$, $\mathbf{i}$, $\mathbf{j}$, $\mathbf{k}$ being unit vectors in the x, y, z directions, respectively, and $R = \sqrt{(x - x_0)^2 + (y - y_0)^2 + z^2}$.

From (2), (5), and (6a)–(6c) the elements of the cross-spectral density matrix at the half space $z > 0$ can be expressed as [21, 25]

$$\begin{aligned} &W_{xx}(\mathbf{r}_1, \mathbf{r}_2) \\ &= \left(\frac{1}{2\pi}\right)^2 \iiiint_{z=0} W_{xx}^0(\mathbf{r}_{01} - 2h_1\mathbf{a}, \mathbf{r}_{02} - 2h_2\mathbf{a}, 0) \\ &\quad \times \frac{\partial}{\partial z}\left[\frac{\exp(-ikR_1)}{R_1}\right] \\ &\quad \times \frac{\partial}{\partial z}\left[\frac{\exp(ikR_2)}{R_2}\right] dx_{01}\, dx_{02}\, dy_{01}\, dy_{02}, \end{aligned} \tag{7a}$$

$$\begin{aligned} &W_{zz}(\mathbf{r}_1, \mathbf{r}_2) \\ &= \left(\frac{1}{2\pi}\right)^2 \iiiint_{z=0} W_{xx}^0(\mathbf{r}_{01} - 2h_1\mathbf{a}, \mathbf{r}_{02} - 2h_2\mathbf{a}, 0) \\ &\quad \times \frac{\partial}{\partial x_1}\left[\frac{\exp(-ikR_1)}{R_1}\right] \\ &\quad \times \frac{\partial}{\partial x_2}\left[\frac{\exp(ikR_2)}{R_2}\right] dx_{01}\, dx_{02}\, dy_{01}\, dy_{02}, \end{aligned} \tag{7b}$$

$$W_{xz}(\mathbf{r}_1, \mathbf{r}_2) = -\left(\frac{1}{2\pi}\right)^2 \iiiint_{z=0} W_{xx}^0(\mathbf{r}_{01} - 2h_1\mathbf{a}, \mathbf{r}_{02} - 2h_2\mathbf{a}, 0)$$

$$\times \frac{\partial}{\partial z}\left[\frac{\exp(-ikR_1)}{R_1}\right]$$

$$\times \frac{\partial}{\partial x_2}\left[\frac{\exp(ikR_2)}{R_2}\right] dx_{01}\,dx_{02}\,dy_{01}\,dy_{02}, \tag{7c}$$

$$W_{xy}(\mathbf{r}_1,\mathbf{r}_2) = W_{yx}(\mathbf{r}_1,\mathbf{r}_2) = W_{yy}(\mathbf{r}_1,\mathbf{r}_2) = 0. \tag{7d}$$

On substituting from (5) into (6a)–(6c), tedious but straightforward integral calculations yield

$$W_{xx}(\mathbf{r}_1,\mathbf{r}_2,z) = \sum_{h_1=-\frac{1}{2}}^{\frac{1}{2}}\sum_{h_2=-\frac{1}{2}}^{\frac{1}{2}} \frac{E_{01}E_{02}\pi^2 z^2}{2A^2B^3r_1^3r_2^2\lambda^2\sigma_0^2}$$
$$\times \left\{2r_1\left[B + g_1^2 + g_2^2 - 2aBh_2(g_1 - ig_2)\right]\right.$$
$$+ B\sigma_0^2(2aBh_2 - g_1 - ig_2)$$
$$\left.\times (4aAh_1r_1 - 2mr_1 - ky_1)\right\}\exp(\Psi), \tag{8a}$$

$$W_{xz}(\mathbf{r}_1,\mathbf{r}_2,z) = \sum_{h_1=-\frac{1}{2}}^{\frac{1}{2}}\sum_{h_2=-\frac{1}{2}}^{\frac{1}{2}} -\frac{E_{01}E_{02}\pi^2 z}{4A^2B^4r_1^3r_2^2\lambda^2\sigma_0^2}$$
$$\times \left\{4r_1\left[(Bx_2 - g_1)\left(g_1^2 + g_2^2\right)\right.\right.$$
$$+ 2Bg_1\left(ah_2(g_1 - ig_2) - 1\right)$$
$$\left.+ B^2\left(x_2 + ah_2(1 - 2g_2x_2 + 2ig_2x_2)\right)\right]$$
$$+ B\sigma_0^2(4aAh_1r_1 - 2mr_1 - ky_1)$$
$$\times \left[2g_1(g_1 + ig_2) + B - 2Bx_2(g_1 + ig_2)\right.$$
$$\left.\left. - 4aBh_2(g_1 - Bx_2)\right]\right\}\exp(\Psi), \tag{8b}$$

$$W_{zz}(\mathbf{r}_1,\mathbf{r}_2,z) = \sum_{h_1=-\frac{1}{2}}^{\frac{1}{2}}\sum_{h_2=\frac{1}{2}}^{\frac{1}{2}} \frac{E_{01}E_{02}\pi^2}{AB\lambda^2r_1^2r_2^2}$$
$$\times \left[\frac{V_1}{2B}\left(1 + \frac{2g_2^2}{B}\right) + \frac{V_2g_2}{B} + V_3\right]\exp(\Psi), \tag{8c}$$

where

$$A = \frac{1}{w_0^2} + \frac{1}{\sigma_0^2} + \frac{ik}{2r_1},$$
$$B = \frac{1}{w_0^2} + \frac{1}{\sigma_0^2} - \frac{ik}{2r_2} - \frac{1}{A\sigma_0^4}, \tag{9}$$

$$g_1 = \frac{ikx_1}{2Ar_1\sigma_0^2} - \frac{ikx_2}{2r_2}, \qquad g_2 = \frac{iky_1}{2Ar_1\sigma_0^2} - \frac{iky_2}{2r_2}, \tag{10}$$

$$m = \frac{2ah_1}{w_0^2} + \frac{ikx_1}{2r_1} + \frac{2a}{\sigma_0^2}(h_1 - h_2), \tag{11}$$

$$\Psi = ik(r_2 - r_1) + \frac{g_1^2 + g_2^2}{B} - \frac{4a(h_1^2 + h_2^2)}{w_0^2}$$
$$- \frac{4a^2(h_1 - h_2)^2}{\sigma_0^2} + \frac{m^2 + (\frac{iky_1}{2r_1})^2}{A}, \tag{12}$$

$$V_1 = \frac{2g_1^2 + B[1 - 2g_1x_2 + 2\sigma_0^2(m - Ax_1)(g_1 - Bx_2)]}{2A^2B^2\sigma_0^4}, \tag{13}$$

$$V_2 = \frac{i}{4A^2B^2r_1\sigma_0^4}\left\{\sigma_0^2\left(B + 2g_1^2 - 2Bg_1x_2\right)(2mr_1 + ky_1)\right.$$
$$- 2B\sigma_0^4(Bx_2 - g_1)\left[r_1\left(A + 2m^2 - 2Amx_1\right)\right.$$
$$\left.+ ky_1(m - Ax_1)\right] + 4ar_1\left(h_2 - Ah_1\sigma_0^2\right)\left[2g_1^2 + B\right.$$
$$\left.\left. - 2Bg_1x_2 + 2B\sigma_0^2(m - Ax_1)(g_1 - Bx_2)\right]\right\}, \tag{14}$$

$$V_3 = \frac{1}{4A^2B^4r_1\sigma_0^4}\left\{r_1\left[4g_1^4 + 4aB^3h_2x_2\right.\right.$$
$$- 4Bg_1^2(-6 + 2ag_1h_2 + g_1x_2) + 3B^2 - 6B^2g_1x_2$$
$$+ 4B^2ag_1h_2(2g_1x_2 - 3)\left.\right] - B\sigma_0^2(4aAh_1r_1 - 4mr_1$$
$$+ 2Ar_1x_1 - ky_1)\left[2g_1^3 + Bg_1\left(3 - 2g_1(2ah_2 + x_2)\right)\right.$$
$$+ B^2\left(2ah_2(2g_1x_2 - 1) - x_2\right)\left.\right] + B^2\sigma_0^4\left[2g_1^2 + B\right.$$
$$\left. - 2Bg_1x_2 - 4aBh_2(g_1 - Bx_2)\right]\left[r_1(A - 4aAmh_1\right.$$
$$\left.\left.+ 2m^2 - 2Ax_1(m - 2aAh_1)\right) + ky_1(m - Ax_1)\right]\right\}. \tag{15}$$

In the above derivations the approximation

$$\frac{\partial}{\partial x}\left[\frac{\exp(ikR)}{R}\right] \approx ik\frac{(x - x_0)}{R^2}\exp(ikR), \tag{16}$$

was used, which holds true for $R_v \gg \lambda$ [25].

Equations (8a)–(8c) indicate that the 3×3 cross-spectral density matrix in the z plane contains only four elements W_{xx}, W_{zz}, W_{xz}, and W_{zx}. In comparison to (2), due to the nonparaxial free-space propagation, the z component W_{zz}, and the correlation terms W_{xz}, W_{zx} appear. As a result, the linear polarization becomes elliptical in the nonparaxial case. Such a type of beam has the peculiar property that all polarization ellipses line in planes parallel to the xz plane where the z axis is along the propagation direction, which is different from the paraxial case where for elliptically polarized light the polarization ellipses all line in planes perpendicular to the propagation direction. Therefore, in analogy to [12, 26], with a suitable change in the definition of the spectral Stokes parameters, the spectral Stokes singularities can be extended from the paraxial regime to the nonparaxial one.

On placing $r_1 = r_2 = r$, $x_1 = x_2 = x$, $y_1 = y_2 = y$ into (8a)–(8c), the spectral Stokes parameters can be defined as

$$S_0(x,y,z) = W_{zz}(x,y,z) + W_{xx}(x,y,z), \tag{17a}$$

$$S_1(x,y,z) = W_{zz}(x,y,z) - W_{xx}(x,y,z), \tag{17b}$$

$$S_2(x,y,z) = W_{zx}(x,y,z) + W_{xz}(x,y,z), \tag{17c}$$

$$S_3(x,y,z) = i\big[W_{xz}(x,y,z) - W_{zx}(x,y,z)\big], \tag{17d}$$

where $W_{zx}(x,y,z) = W^*_{xz}(x,y,z)$. The normalized spectral Stokes parameters are $s_1 = S_1/S_0$, $s_2 = S_2/S_0$ and $s_3 = S_3/S_0$.

The complex spectral Stokes fields s_{ij} ($i,j = 1,2,3$ unless otherwise stated) are given by [7]

$$s_{12} = s_1 + is_2, \tag{18a}$$

$$s_{23} = s_2 + is_3, \tag{18b}$$

$$s_{31} = s_3 + is_1, \tag{18c}$$

and the degree of polarization is

$$P = \sqrt{s_1^2 + s_2^2 + s_3^2}. \tag{19}$$

Similar to their counterparts in fully coherent nonparaxial wavefields [18], the composite spectral Stokes singularities (vortices) correspond to the zero points (phase singularities) of complex Stokes fields $s_{ij} = 0$ in partially coherent nonparaxial wavefields. s_{12} singularities correspond to the circular polarization (C-points), and $s_3 > 0$ ($s_3 < 0$) means right- (left-) handedness, where the orientation of the major and minor axes of the polarization ellipse becomes undefined. s_{23} and s_{31} singularities must be located on L-lines, where the handedness of the polarization ellipse is undetermined (linear polarization). From (8), (17), and (18), it is readily seen that the composite spectral Stokes singularities depend on the controlling parameters, including the spatial correlation length σ_0, the waist width w_0 (or ratio of waist width to wavelength w_0/λ), and the off-axis distance a, and on the propagation distance z. In the fully coherent limit ($\sigma_0 \to \infty$) the composite Stokes singularities degenerate into the composite polarization singularities.

3 Composite spectral Stokes singularities in a fixed plane

From Sect. 2 we see that the composite spectral Stokes singularities in a fixed plane are dynamically variable if a controlling parameter, such as the spatial correlation length σ_0, the ratio of waist width to wavelength w_0/λ, or the off-axis distance a, is changed which can be illustrated numerically by using (8), (17), and (18).

3.1 Dependence of s_{12}, s_{23}, and s_{31} singularities on the spatial correlation length

Figures 1a–e give s_{12}, s_{23}, and s_{31} singularities in the plane $z = 30\lambda$ for different values of the spatial correlation length (a) $\sigma_0 = 2\lambda$, (b) $\sigma_0 = 2.2\lambda$, (c) $\sigma_0 = 2.34211\lambda$, (d) $\sigma_0 = 2.5\lambda$, (e) $\sigma_0 = 2.9\lambda$, $w_0 = 0.5\lambda$, $a = 4.5\lambda$, and $\lambda = 1$ μm. The contours of $s_1 = 0$, $s_2 = 0$, and $s_3 = 0$ are represented by the solid, dashed, and dotted curves, respectively. s_{12} (C-points), s_{23}, and s_{31} singularities appear at the intersection of $s_i = 0$ and $s_j = 0$, and are represented by the circles, triangles, and squares, the black and open ones correspond to the topological charges $m_{ij} = -1$ and $+1$, respectively, which are determined by the sign principle [6, 27]. The L-lines ($s_3 = 0$) separate the xy plane into the right- and left-handed regions [12, 18], and the signs $\pm$ of s_3 determine the handedness of C-points and are shown in the figures. As can be seen, for $\sigma_0 \le 2.3\lambda$ in Figs. 1a, 1b there are no C-points in the region $\{17.1 \le x/\lambda \le 18.6, -10 \le y/\lambda \le 10\}$. For $\sigma_0 = 2.34211\lambda$ in Fig. 1c a pair of C-points marked 1 and 2 with opposite topological charge but same right-handedness are present, which are located at $(17.620, 4.381)$, $(17.621, 4.381)$, and their degree of polarization $P = 0.005$, 0.002, respectively. With a slight increase of the spatial correlation length to $\sigma_0 = 2.34213\lambda$ C-point 2 moves to the L-line at $(17.621, 4.382)$ and collides with it (not shown). At such critical point $\sigma_{0C} = 2.34213\lambda$ the intensity is equal to zero because $S_1 = S_2 = S_3 = S_0 = 0$. It means that the collision of C-point 2 and L-line leads to a V-point [12] at which the degree of polarization $P = 0$ sometimes called the U-singularity [14, 17]. The V-point is unstable because a small perturbation of σ_0 results in the handedness reversal and changes in the degree of polarization of C-point 2. For example, for $\sigma_0 = 2.34216\lambda$ C-point 2 shifts to $(17.622, 4.382)$ and becomes left-handed whose degree of polarization $P = 0.003$. For $\sigma_0 = 2.38993\lambda$ a pair of C-points 3 and 4 with opposite topological charge but same handedness and $P = 0.006$, 0.001 appear. In the vicinity of the critical point $\sigma_{0C} = 2.38994\lambda$ the handedness of C-point 4 is reversed (not shown). When σ_0 is increased to $\sigma_0 = 2.5\lambda$ in Fig. 1d C-points 1, 2, 3, 4 move to $(17.538, 4.180)$, $(17.673, 4.299)$, $(17.363, -4.548)$, $(17.473, -4.652)$ and $P = 0.323$, 0.321, 0.278, 0.271, respectively. With a further increase to $\sigma_0 = 2.9\lambda$ in Fig. 1e, C-points 1, 2, 3, 4 shift to $(17.465, 3.879)$, $(17.690, 4.048)$, $(17.297, -4.283)$, $(17.509, -4.452)$ and their degree of polarization P becomes 0.561, 0.554, 0.542, 0.535, respectively.

There exist a pair of oppositely charged s_{23} singularities marked A and B for $\sigma_0 = 2\lambda$ in Fig. 1a, whose position is $(17.945, 6.969)$, $(17.707, -7.573)$ and $P = 0.126$, 0.149, respectively. With increasing σ_0, their motion and changes in the degree of polarization take place, for example, for $\sigma_0 = 2.5\lambda$ in Fig. 1d A and B move to $(17.515, 3.261)$, $(17.378, -3.904)$ and $P = 0.553$, 0.04, respectively. When σ_0 is increased to $\sigma_0 = 2.9\lambda$ in Fig. 1e s_{23} singularities A and B annihilate each other.

A pair of oppositely charged s_{31} singularities labeled a and b are present for $\sigma_0 = 2.2\lambda$ in Fig. 1b, which are lo-

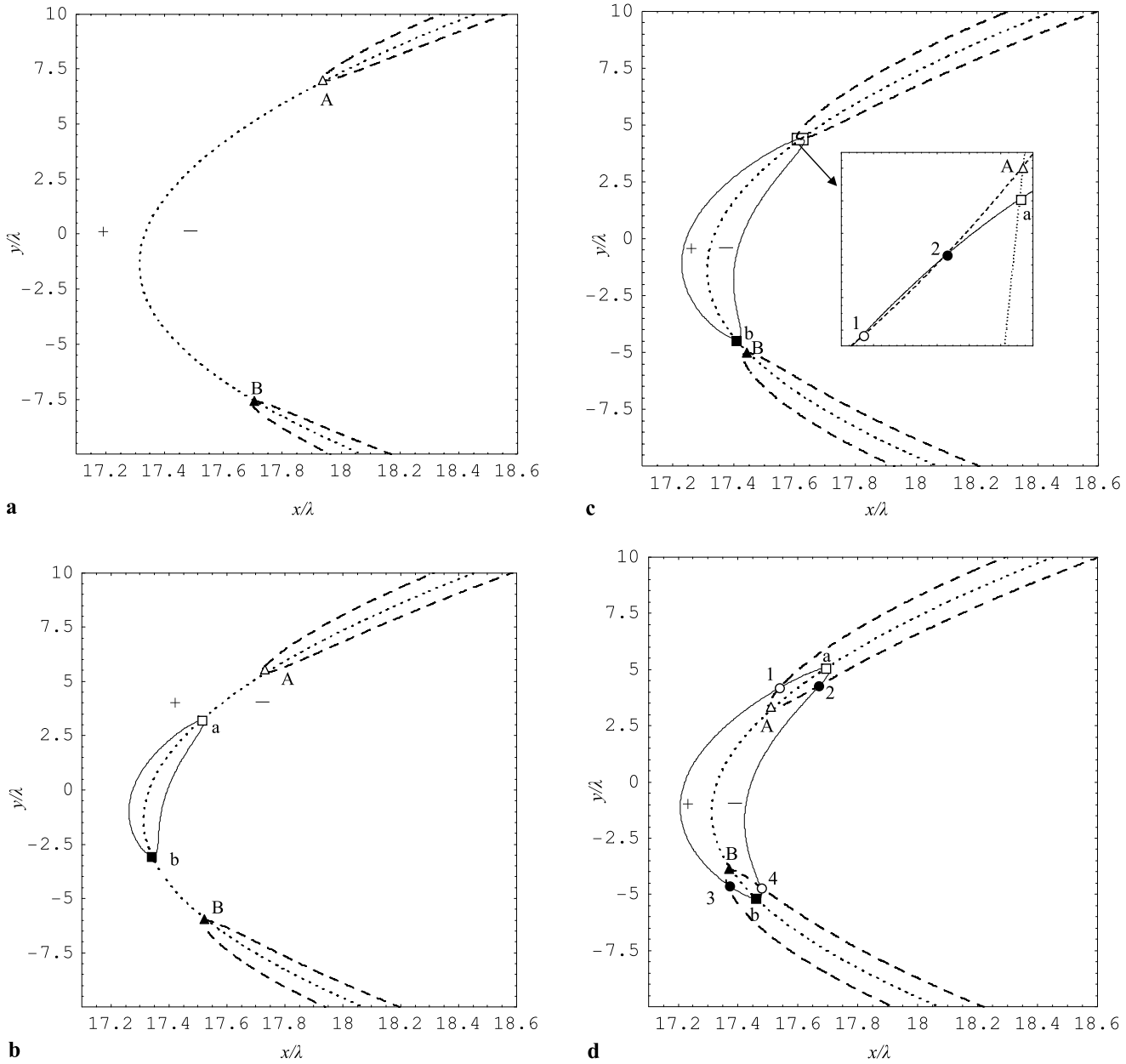

Fig. 1 s_{12}, s_{23}, and s_{31} singularities for different values of the spatial correlation length σ_0, (**a**) $\sigma_0 = 2\lambda$, (**b**) $\sigma_0 = 2.2\lambda$, (**c**) $\sigma_0 = 2.34211\lambda$, (**d**) $\sigma_0 = 2.5\lambda$, (**e**) $\sigma_0 = 2.9\lambda$. The other calculation parameters are seen in the text

cated at $(17.511, 3.208)$, $(17.341, -3.033)$ and $P = 0.108$, 0.137, respectively. With increasing σ_0, singularities a and b move and their degree of polarization changes. For example, for $\sigma_0 = 2.9\lambda$ in Fig. 1e s_{31} singularities a and b shift to $17.8, 5.930)$, $(17.548, -6.167)$ and $P = 0.279, 0.256$, respectively.

To illustrate the variation of a composite spectral Stokes singularity with the correlation length σ_0, we choose C-point 1 in Fig. 1 as an example. Figure 2 shows the correction between the composite spectral Stokes singularity of partially coherent beams and the composite Stokes singularity of their counterparts in the fully coherent case. It is seen that when the correlation length σ_0 is decreased, the composite spectral Stokes singularity moves away from the composite Stokes singularity ($\sigma_0 \to \infty$), whereas with increasing σ_0 the composite spectral Stokes singularity approaches to the composite Stokes singularity, e.g., for $\sigma_0 = 10\lambda$, 15λ, 30λ, and 50λ the position of C-point is $(17.314, 3.038)$, $(17.307, 2.990)$, $(17.303, 2.962)$ and $(17.302, 2.956)$, respectively, and finally becomes the composite Stokes singularity located at $(17.301, 2.952)$ when $\sigma_0 \geq 200\lambda$. The evolution behavior of the composite spectral Stokes singu-

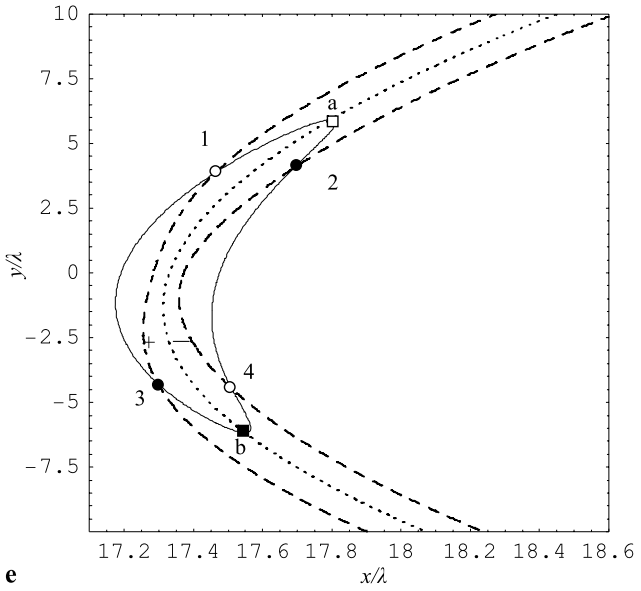

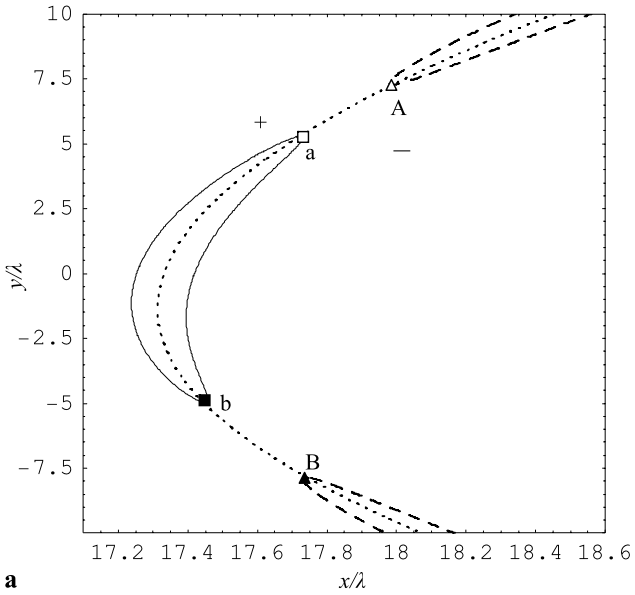

Fig. 1 (*Continued*)

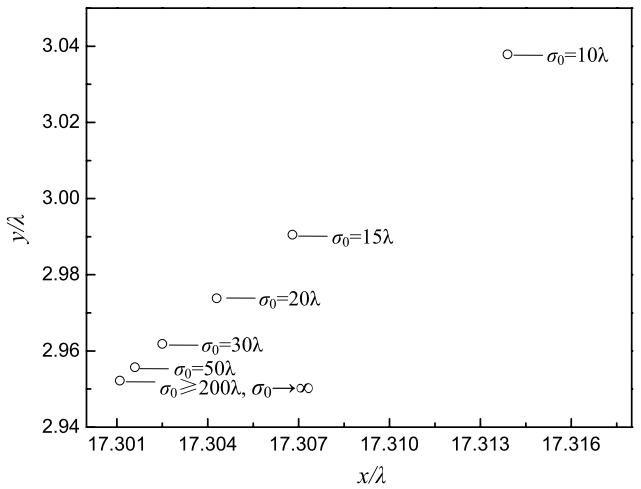

Fig. 2 Evolution of a composite spectral Stokes singularity into a composite Stokes singularity

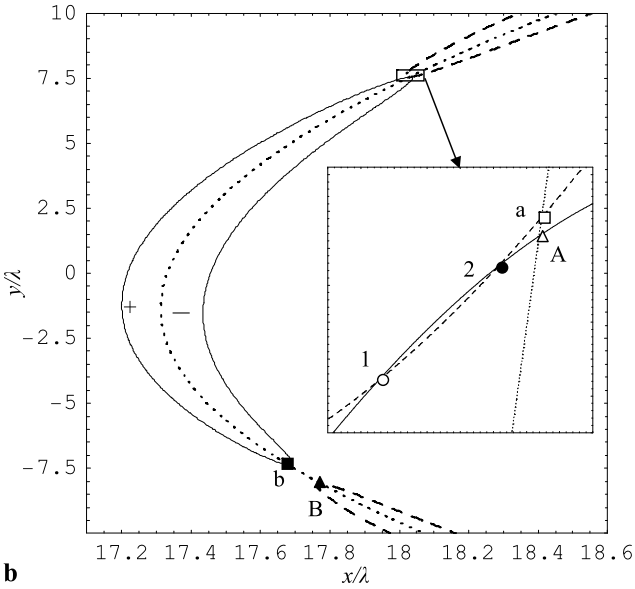

Fig. 3 s_{12}, s_{23}, and s_{31} singularities for different values of the ratio of the waist width to the wavelength w_0/λ, (**a**) $w_0/\lambda = 0.49$, (**b**) $w_0/\lambda = 0.483128$

larities is physically similar to that of the coherence vortices [29].

3.2 Dependence of s_{12}, s_{23}, and s_{31} singularities on the ratio of waist width to wavelength

s_{12}, s_{23}, and s_{31} singularities in the plane $z = 30\lambda$ for different values of w_0/λ are plotted in Fig. 3 (a) $w_0/\lambda = 0.49$, and (b) $w_0/\lambda = 0.483128$, and the other calculation parameters are the same as those in Fig. 1a. It is seen that for $w_0/\lambda = 0.49$ in Fig. 3a no C-points are present. If w_0/λ is decreased to $w_0/\lambda = 0.483128$ in Fig. 3b a pair of C-points 1, 2 with the opposite topological charge but the same right handedness appear, which are located at $(18.027, 7.538)$, $(18.028, 7.539)$ and $P = 0.006, 0.001$. At the critical point of $w_{0C}/\lambda = 0.4831275$ (not shown) C-point 2 shifts to $(18.029, 7.539)$ and coincides with the V-point. With a slight decrease to $w_0/\lambda = 0.483125$, C-point 2 moves to $(18.029, 7.540)$, and its handedness is reversed and $P = 0.004$. In addition, as compared with Fig. 1a, the creation of s_{31} singularities a and b, the motion and changes in the degree of polarization of s_{23} and s_{31} singularities A, B and a, b are also observed in Figs. 3a and 3b.

It is noted that we take $w_0/\lambda \approx 0.5$ to satisfy the nonparaxial approximation. As shown in Fig. 4, where $I_{z,\max}(x, 0, 30\lambda)/I_{\max}(x, 0, 30\lambda)$ is depicted versus w_0/λ, $I_{z,\max}(x, 0, 30\lambda)$ and $I_{\max}(x, 0, 30\lambda)$ denote the maximum

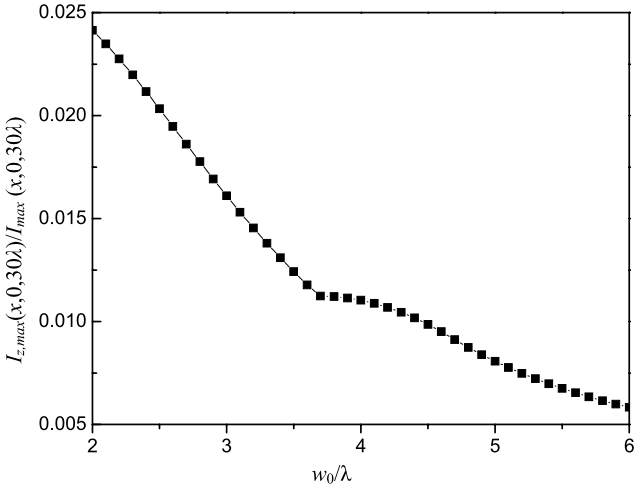

Fig. 4 $I_{z,\max}(x,0,30\lambda)/I_{\max}(x,0,30\lambda)$ versus w_0/λ

longitudinal intensity and the maximum total intensity [28], respectively, and $\sigma_0 = 5\lambda$, $z = 30\lambda$. $I_{z,\max}(x,0,30\lambda)/I_{\max}(x,0,30\lambda)$ decreases with increasing w_0/λ. For $w_0/\lambda = 6$ $I_{z,\max}(x,0,30\lambda)/I_{\max}(x,0,30\lambda) < 0.6\%$. In the extreme paraxial region the longitudinal electric-field component disappears, thus the partially coherent beams described by (6a)–(6c) degenerate into scalar ones so that polarization singularities are absent.

Similar behavior of composite spectral Stokes singularities is present by varying the off-axis distance a and is omitted here.

4 Propagation of composite spectral Stokes singularities in free space

The dynamic evolution of s_{12}, s_{23}, and s_{31} singularities in free space is described in (8), (17), and (18) by varying the propagation distance z. Figures 5a–d show s_{12}, s_{23}, and s_{31} singularities for different values of the propagation distance (a) $z = 15\lambda$, (b) $z = 15.7\lambda$, (c) $z = 18\lambda$, (d) $z = 34.646\lambda$, and $w_0 = 0.5\lambda$, $a = 3.9\lambda$, $\sigma_0 = 2\lambda$. From Fig. 5a we see that in the region $\{7.4 \le x/\lambda \le 9.8, -7 \le y/\lambda \le 7\}$ these are C-points 1, 2 with opposite topological charge and handedness located at $(8.013, 4.230)$, $(8.108, 4.296)$ and $P = 0.222$, 0.216, respectively. With increasing z, the motion and changes in degree of polarization of C-points 1, 2 are observed. For example, at $z = 15.7\lambda$ in Fig. 5b C-points 1, 2 move to $(8.381, 4.467)$, $(8.476, 4.535)$ and $P = 0.223$, 0.217. At $z = 18\lambda$ in Fig. 5c C-points 1, 2 shift to $(9.591, 5.236)$, $(9.688, 5.308)$ and their degree of polarization becomes $P = 0.227$, 0.220, respectively. As z is increased to $z = 34.646\lambda$ in Fig. 5d s_{12}, s_{23}, and s_{31} singularities are not found in the region $\{7.4 \le x/\lambda \le 9.8, -7 \le y/\lambda \le 7\}$, C-points 1, 2 move to $(18.362, 10.628)$, $(18.456, 10.705)$ and in the region $\{17.2 \le x/\lambda \le 18.6, -12 \le y/\lambda \le 12\}$ a pair of C-points 3, 4 with opposite topological charge but same right-handedness appear, which are located at $(18.037, -10.901)$, $(18.037, -10.902)$, $P = 0.003$, 0.001, respectively. In the vicinity of the critical point of $z_C = 34.648\lambda$, the handedness reversal of C-point 4 can be observed.

The motion and changes in the degree of polarization of s_{23} singularities are present in the free-space propagation. For example, at $z = 15.7\lambda$ in Fig. 5b a pair of oppositely charged s_{23} singularities A and B are located at $(8.411, 4.380)$, $(8.035, -4.854)$ and $P = 0.023$, 0.032, and at $z = 18\lambda$ in Fig. 5c A and B move to $(9.617, 5.125)$, $(9.257, -5.618)$ and $P = 0.023$, 0.023, respectively.

The free-space propagation results in the motion, creation, annihilation, and changes in the degree of polarization of s_{31} singularities. For example, as compared with Figs. 5a and 5b, a pair of oppositely charged s_{31} singularities a and b move from $(8.104, 4.538)$, $(7.621, 0.646)$ to $(8.474, 4.787)$, $(7.949, 0.438)$ and their degree of polarization is changed from $P = 0.072$, 0.521 to 0.071, 0.526, respectively. A pair of s_{31} singularities c and d with opposite topological charge with $P = 0.351, 0.198$ in Fig. 5b appear at the position $(7.854, -2.853)$, $(7.916, -3.782)$, respectively. With increasing to $z = 18\lambda$ in Fig. 5c s_{31} singularities b and c with opposite topological charge annihilate each other.

It can be verified that the topological relationship between the topological charges of the polarization singularities [7, 16]

$$2\sigma_k \sum\nolimits_{(k)} m_{ij} = \sum\nolimits^{(k)} \sigma_i m_{jk} = \sum\nolimits^{(k)} \sigma_j m_{ik}, \tag{20}$$

holds true for the composite spectral Stokes singularities in partially coherent nonparaxial wavefields, where $\sum_{(k)}$ denotes the summation over the composite spectral Stokes singularities contained within a closed contour of $s_k = 0$, and $\sum^{(k)}$ denotes the summation over the composite spectral Stokes singularities on the contour. $\sigma_{i,j,k} = 1$ and -1 for $s_{i,j,k} > 0$ and $s_{i,j,k} < 0$, respectively. m_{ij} is the topological charge of s_{ij} singularities and the order of the indices of m_{ij} is a cyclic permutation of 1, 2, and 3. For example, there is a closed solid curve ($s_1 = 0$) in Fig. 1d. We have $2\sigma_k \sum_{(k)} m_{ij} = 2 \times [(-1) \times (+1) + (-1) \times (-1)] = 0$ and $\sum^{(k)} \sigma_i m_{jk} = (+1) \times (+1) + (-1) \times (-1) + (+1) \times (-1) + (-1) \times (+1) = 0$, $\sum^{(k)} \sigma_j m_{ik} = (-1) \times (+1) + (-1) \times (-1) = 0$.

5 Conclusion

In this paper, the composite spectral Stokes singularities have been introduced to describe polarization singulari-

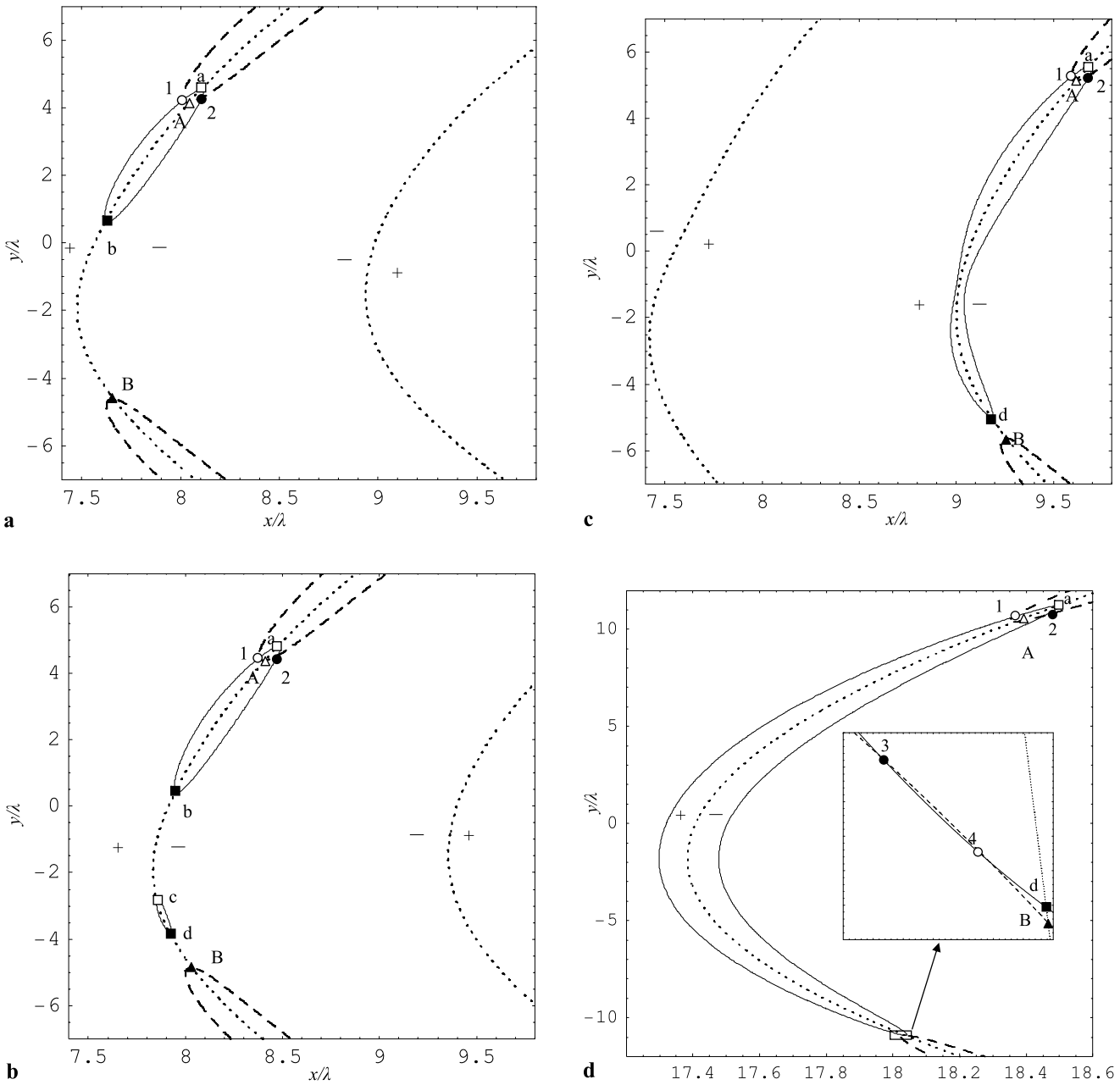

Fig. 5 s_{12}, s_{23}, and s_{31} singularities for different values of the propagation distance z, (**a**) $z = 15\lambda$, (**b**) $z = 15.7\lambda$, (**c**) $z = 18\lambda$, (**d**) $z = 34.646\lambda$

ties in superimposed partially coherent beams beyond the paraxial approximation. Based on the vector Rayleigh–Sommerfeld diffraction integrals, the analytical expression for the cross-spectral density matrix has been derived, which enables us to study the dynamic behavior of composite spectral Stokes singularities. Our study has shown the existence of s_{12}, s_{23}, and s_{31} composite spectral Stokes singularities. The motion, creation and annihilation, and changes in the degree of polarization of s_{12}, s_{23}, and s_{31} singularities as well as the handedness reversal of s_{12} singularities may appear in the variation of a controlling parameter, such as the spatial correlation length σ_0, ratio of the waist width to the wavelength w_0/λ, or the off-axis distance a, or in the variation of the propagation distance z. The creation and annihilation take place for a pair of s_{12} singularities with opposite topological charge but same handedness, and for a pair of oppositely charged s_{23} and s_{31} singularities. There exists the critical point of the controlling parameters and the propagation distance, where the collision of an s_{12} singularity (C-point) and an L-line takes place resulting in a V-point (U singularity), which is unstable. A small perturbation leads to the handedness reversal and changes in the

degree of polarization of the C-point. For composite spectral Stokes singularities in partially coherent nonparaxial wavefields the topological relationship holds still true.

As compared with [16, 18], where the spectral Stokes singularities of partially coherent electromagnetic beams in the paraxial approximation and the composite polarization singularities in superimposed fully coherent nonparaxial beams were analyzed, respectively, in this paper the composite spectral Stokes singularities in superimposed partially coherent beams beyond the paraxial approximation have been studied, where both the partial coherence and the nonparaxility of beams have been taken into consideration, and the dependence of composite spectral Stokes singularities on the spatial correlation and the dynamic evolution of composite spectral Stokes singularities in the nonparaxial propagation have been stressed. In particular, the conventional spectral Stokes parameters used in [16] should be extended and the generalized Rayleigh–Sommerfeld diffraction integrals should be used to meet our theoretical formulation, and the propagation of the cross-spectral density matrix instead of the electric-field components in [18] should be treated, thus some richer dynamic behavior of the composite spectral Stokes singularities in the partially coherent nonparaxial regime can be observed.

As a nonparaxial eigenmode of stable resonators [30], the LG (0, 1) beam described by (1a)–(1b) ($n = 1$) can be generalized by using the mode selection techniques. Then, by passing the beam through a random phase screen, the partially coherent LG (0, 1) beam in (4) can be obtained [22]. The free-space propagation of such beam should be nonparaxial because its waist width w_0 is the order of the wavelength (e.g., $w_0 = 0.5\lambda$) [31]. The verification of the phenomena described in this paper theoretically requires the precise experimental measurement in a subwavelength scale. Such measurement may be realized by using the interferometric nanoprobe techniques [10]. The results obtained in this paper would be useful for a deep understanding of composite polarization singularities in superimposed partially coherent nonparaxial wavefields and for their controlling.

Acknowledgements This work was supported by the National Natural Science Foundation of China (NSFC) under grant No. 10874125 and the Natural Science Foundation of Luzhou Medical College. The authors are grateful to the anonymous reviewer for the insightful comments and valuable suggestions which were useful for improving the quality of this paper.

References

1. J.F. Nye, *Natural Focusing and the Fine Structure of Light* (IOP Publishing, Bristol, 1999)
2. J.F. Nye, J.V. Hajnal, Proc. R. Soc. Lond. A **409**, 21 (1987)
3. J.V. Hajnal, Proc. R. Soc. Lond. A **430**, 413 (1990)
4. M.V. Berry, M.R. Dennis, Proc. R. Soc. Lond. A **457**, 141 (2001)
5. I. Freund, Opt. Commun. **201**, 251 (2002)
6. A.I. Mokhun, M.S. Soskin, I. Freund, Opt. Lett. **27**, 995 (2002)
7. I. Freund, A.I. Mokhun, M.S. Soskin, O.V. Angelsky, I.I. Mokhun, Opt. Lett. **27**, 545 (2002)
8. O.V. Angelsky, I.I. Mokhun, A.I. Mokhun, M.S. Soskin, Phys. Rev. E **65**, 036602(5) (2002)
9. M.S. Soskin, V. Denisenko, I. Freund, Opt. Lett. **28**, 1475 (2003)
10. M.S. Soskin, V.G. Denisenko, R.I. Egorov, Proc. SPIE **5458**, 79 (2004)
11. F. Flossmann, U.T. Schwarz, M. Maier, M.R. Dennis, Phys. Rev. Lett. **95**, 253901(4) (2005)
12. R.W. Schoonover, T.D. Visser, Opt. Express **14**, 5733 (2006)
13. M.R. Dennis, Opt. Lett. **33**, 2572 (2008)
14. C.V. Felde, A.A. Chernyshov, G.V. Bogatyryova, P.V. Polyanskii, M.S. Soskin, JETP Lett. **88**, 418 (2008)
15. K.Y. Bliokh, A. Niv, V. Kleiner, E. Hasman, Opt. Express **16**, 695 (2008)
16. H. Yan, B. Lü, Opt. Lett. **34**, 1933 (2009)
17. A.A. Chernyshov, Ch.V. Felde, H.V. Bogatyryova, P.V. Polyanskii, M.S. Soskin, J. Opt. A: Pure Appl. Opt. **11**, 094010(8) (2009)
18. Y. Luo, B. Lü, J. Opt. Soc. Am. A **27**, 578 (2010)
19. O. Korotkova, E. Wolf, Opt. Lett. **30**, 198 (2005)
20. I.D. Maleev, G.A. Swartzlander Jr., J. Opt. Soc. Am. B **20**, 1169 (2003)
21. L. Mandel, E. Wolf, *Optical Coherence and Quantum Optics* (Cambridge University Press, Cambridge, 1995)
22. M. Zahid, M.S. Zubairy, Opt. Commun. **70**, 361 (1989)
23. B. Li, B. Lü, J. Opt. A: Pure Appl. Opt. **5**, 303 (2003)
24. R.K. Luneburg, *Mathematical Theory of Optics* (University of California Press, Berkeley, 1966)
25. K. Duan, B. Lü, J. Opt. Soc. Am. A **21**, 1924 (2004)
26. Y. Zhu, D. Zhao, Phys. Rev. A **373**, 1595 (2009)
27. I. Freund, N. Shvartsman, Phys. Rev. A **50**, 5164 (1994)
28. K. Duan, B. Lü, J. Opt. Soc. Am. A **21**, 1613 (2004)
29. G. Gbur, T.D. Visser, E. Wolf, J. Opt. A: Pure Appl. Opt. **6**, S239 (2004)
30. H. Laabs, A.T. Friberg, IEEE J. Quantum Electron. **35**, 198 (1999)
31. S. Nemoto, Appl. Opt. **29**, 1940 (1990)